JOURNAL OF MATERIALS SCIENCE 37 (2002) 4369–4377

Crystallization behavior of calcium phosphate glass powder

M. B. TOŠIĆ
Institute for Technology of Nuclear and other Mineral Raw Materials, 86 Franchet d' Esperey, 11000 Belgrade, Yugoslavia
E-mail: m.tosic@itnms.ac.yu

R. Ž. DIMITRIJEVIĆ
Faculty of Mining and Geology, University of Belgrade, 7 Djušina, 11000 Belgrade, Yugoslavia

M. M. MITROVIĆ
Faculty of Physics, University of Belgrade, 12-16 Akademski Trg, 11000 Belgrade, Yugoslavia

N. S. BLAGOJEVIĆ
Faculty of Technology and Metallurgy, 4 Karnegijeva St.,11000 Belgrade, Yugoslavia

The crystallization behavior of calcium phosphate glass powder with the molar ratio $[CaO]/[P_2O_5] = 0.88$, to which 6.38 mol% TiO_2 and 10 mol% Al_2O_3 were added as nucleation agents, was investigated. The results indicate complex crystallization behavior which depends on the powder particle size and the crystallization temperature. In the crystallization temperature range $T_c < 900^\circ C$ the surface mechanism of crystallization dominates in the case of all particle sizes ranging from 0–1 mm and the β-$Ca_2P_2O_7$ phase is formed. At very long annealing times volume crystallization occurs and the TiP_2O_7 and $AlPO_4$ phases are formed. In the temperature interval $T_c > 900^\circ C$ the dominant crystallization mechanism depends on the particle size. In the size range 0.15–0.5 mm the surface mechanism of crystallization is replaced by the volume one. In the range >0.5 mm the volume mechanism of crystallization is dominant. The phases β-$Ca_2P_2O_7$, TiP_2O_7 and $AlPO_4$ are formed in that temperature interval for all particle sizes. The additives TiO_2 and Al_2O_3 influence the nucleation and formation of TiP_2O_7 and $AlPO_4$ but do not influence the formation of β-$Ca_2P_2O_7$. © *2002 Kluwer Academic Publishers*

1. Introduction

The basic structural element of phosphate glasses is the $[PO_4]$–tetrahedron. It forms by promoting five external p–electrons ($3s^2\ 3p^3$) to the 3d level causing the formation of an sp^3 hybrid orbital directed toward four oxygen atoms. Under these conditions, strong π-molecular orbitals are formed with oxygen 2p electrons [1]. Such a structural unit has two types of P—O bonds [2]. Three bridging oxygens (BO) are connected by single bonds to the P atom and by them the tetrahedron is connected to neighboring $[PO_4]$–tetrahedra forming P—O—P bonds. The fourth terminal oxygen atom (TO) is connected by a double bond to the P atom (P═O). The length of this bond is considerably shorter, as a consequence of the stronger character of the π–bond. For vitreous P_2O_5 the average lengths for the bridging (BO) and terminal (TO) P—O bonds are 0.158 and 0.143 nm, respectively [3].

Such a bond forms the specific structures of phosphate glasses. Consequently, the behavior of phosphate glasses during crystallization differs in regard to the most commonly used and studied silicate glasses. The structures of phosphate glasses are usually presented using the Q^i terminology where i represents the number of bridging oxygens (BO) per tetrahedron [1]. They start with the three-dimensional network of Q^3 groups, an example of which is vitreous P_2O_5 (v–P_2O_5). Changes in the structure caused by introducing other metallic oxides are most easily followed in the case of binary systems. The addition of modifying oxides leads to the scission of P—O—P bonds and to network depolymerization [2]. Acidic phosphate glasses which contain >50 mol% P_2O_5 also have the structure of a three–dimensional network consisting of Q^3 and Q^2 groups. However, they, like P_2O_5, have poor chemical durability and are, therefore, uninteresting for application. Metaphosphate glasses contain 50 mol% of modifying oxides. They consist of metaphosphate chains or rings formed by Q^2 groups. Their structure is similar to organic polymers. These glasses do not tend to phase separate and thus do not fulfil the criterion required for controlled crystallization [4]. Polyphosphate glasses (inverse phosphate glasses) containing <50 mol% P_2O_5 are formed by further increasing the content of modifying oxides. Their structure consists of chains formed by Q^2 groups and terminate with Q^1 groups.

The average chain length progressively decreases with increasing [O]/[P] ratio: At the ratio [O]/[P] = 3.5 (pyrophosphate stoichiometry—67 mol% of modifying oxides) the structure is dominated by phosphate dimers, two Q^1 groups connected by a bridging oxygen. At [O]/[P] > 3.5 the structures also contain isolated Q° groups (orthophosphate groups) [1]. Due to these reasons polyphosphate glasses exhibit a tendency toward faster structure arrangement—crystallization [4] and are the subject of intensive investigations.

Glasses from the system $CaO–P_2O_5$ are interesting because of their potential application as biomaterials. In general, pure calcium polyphosphate glasses undergo surface crystallization [5]. Watanabe *et al*. [6] have shown that the addition of Al_2O_3 to glass with the molar ratio $[CaO]/[P_2O_5] < 1$ enables their volume crystallization. Hosono *et al*. [7] registered volume crystallization by utilizing the additive TiO_2 in glass with the ratio $[CaO]/[P_2O_5] = 1.35$. Nan *et al*. [8] and Reaney *et al*. [9] used the additives TiO_2 and Al_2O_3 as effective nucleating agents for glasses with the molar ratios $[CaO]/[P_2O_5] \geq 1$. The goal of this paper is the investigation of the crystallization behavior of glass powder with the ratio $[CaO]/[P_2O_5] < 1$ and the additives Al_2O_3 and TiO_2. The investigations were performed under non-isothermal and isothermal crystallization conditions.

2. Experimental

Solid and liquid starting components were used to prepare the mixture for melting. $CaCO_3$, $Al_2O_3 \cdot 3H_2O$ and TiO_2 of reagent grade purity and high-purity quartz (>99.9% SiO_2) were used as solid components, while an aqueous solution of orthophosphoric acid (85 wt% H_3PO_4) was used as the liquid component. The mixture for melting was prepared in the following way:

- mixing and homogenization of the solid components,
- the addition of distilled water and a solution of 85% H_3PO_4 with constant stirring of the mixture,
- drying of the liquid mixture in an electric furnace at $T = 200^\circ$C, and
- pulverization of the dried precipitate and sieving on a 0.83 mesh sieve.

Melting was performed in a Pt crucible in an electric furnace at $T = 1420^\circ$C for $t = 60$ min. The melt was cast on a steel plate and cooled in air. The solidified glass samples were transparent, without residual bubbles, with a purple color typical of glasses containing Ti.

Powder samples of the following granulations: <0.038, 0.038–0.050, 0.050–0.1, 0.1–0.2, 0.2–0.3, 0.3–0.4, 0.4–0.5, 0.5–0.63, 0.63–0.83 and 0.83–1.0 mm, were prepared for the investigations under non-isothermal crystallization conditions. These investigations were performed on a Netsch STA 409 EP instrument. In these experiments a constant sample mass of 100 mg was heated at a rate of $v = 10^\circ$C/min in the temperature interval $T = 25–1100^\circ$C.

Two groups of experiments were performed under isothermal conditions. In the first group of experiments samples of the following granulation: <0.038, 0.1–0.2 and 0.63–0.83 mm, were heated at a rate of $v = 10^\circ$C/min to the temperatures of the corresponding crystallization peaks: $T_p = 800$, 840, 878, 891, 953 and 1004°C, at which they were maintained for $t = 15$ min. In the second group of experiments compact samples were thermally treated in a two–step regime. They were first heated to the nucleation temperature $T_n = 690^\circ$C for $t = 600$ min. Heating was then continued at a rate of $v = 2^\circ$C/min to the chosen crystallization temperature in the range $T_c = 770–1100^\circ$C. When the chosen temperatures T_c were attained, the samples were maintained at these temperatures for various times. After these times the samples were taken out of the furnace and crushed in an agate mortar. Favorable fractions were selected for SEM investigations. The rest of the sample was used for determining the phase composition.

Dilatometric measurements were performed on a sample of 3 mm diameter and 40 mm length, which was heated at a rate of $v = 10^\circ$C/min in the temperature interval $T = 25–700^\circ$C. Before the measurement the sample was pretreated at $T = 630^\circ$C for $t = 30$ min and then slowly cooled at a rate of 1°C/min to 300°C.

The XRD method was used for investigating the phase composition of the crystallized samples. The powder patterns were obtained on a Philips PW—1710 automated diffractometer using experimental conditions described elsewhere [10].

Investigation of the crystal morphology was carried out by scanning electron microscopy using a Jeol JSM 840 A microscope. The samples were gold sputtered in a Jeol JFC 1100 ion sputter.

3. Results and discussion

3.1. The chemical composition of glass

Table I shows the initial composition of the obtained glass and its chemical analysis. It may be seen from Table I that a glass with the ratio $[CaO]/[P_2O_5] = 0.88$ was obtained. According to the results of Reaney *et al*. [9] in the case of glasses with the ratio $[CaO]/[P_2O_5] \geq 1$, the presence of SiO_2 up to 10 mol% does not influence its crystallization and remains amorphous during thermal treatment. Its presence ensures glass formation. For these contents Al_2O_3 and TiO_2 act as modifiers of the phosphate structure [1, 11, 12]. As the content of $CaO + P_2O_5$ is dominant (75.72 mol%), in that case this glass can be considered as the polyphosphate glass $0.56MeO \cdot 0.44P_2O_5$, where $[MeO] = [CaO] + [Al_2O_3] + [TiO_2]$. For this composition the ratio [O]/[P] = 3.15. As the ratio [O]/[P] > 3, the structure of this glass consists of phosphate chains which contain Q^1

TABLE I Composition of the glass

	Composition (mol%)					
Glass	P_2O_5	CaO	Al_2O_3	TiO_2	SiO_2	$[CaO]/[P_2O_5]$
Initial	41	35	10	6	8	0.85
Achieved	40.32	35.40	10.01	6.38	7.89	0.88

and Q^2 tetrahedra. The fractions of Q^1 and Q^2 tetrahedra are 0.27 and 0.73, respectively. The average chain-length (L_{av}) of an anion can be calculated by the formula given by Van Wazer [1]

$$L_{av} = 2(1 - x)/2x - 1 \qquad (1)$$

where x is the molar fraction of MeO. For this polyphosphate glass $L_{av} = 7.3$.

3.2. Determination of dominant mechanisms of crystallization

Investigations of the crystallization of silicate glasses have shown that the particle size of the powder glass influences the mechanism of its crystallization. C. S. Ray *et al.* [13] have proposed a method for evaluating the crystallization mechanism of powder glass. According to this method, the behavior of parameters $(\delta T)_p$ and $T_p^2/(\Delta T)_p$ is determined as a function of the powder particle size, where $(\delta T)_p$ is the height of the DTA peak, T_p is the DTA peak temperature and $(\Delta T)_p$ is the DTA peak width at peak half height. Experimental and theoretical studies have shown that $(\delta T)_p$ is proportional to the total number of nuclei (volume and surface nuclei) contained in the glass [14, 15]. The glasses generally crystallize either by the surface or volume mechanism. Although both crystallization mechanisms can occur simultaneously and competitively, one mechanism usually dominates. For dominant surface crystallization or negligible volume crystallization, a decrease in $(\delta T)_p$ should be observed with increasing particle size, because the total effective surface area of the glass particles decreases and hence, the number of surface nuclei decreases with increasing particle size. When volume nucleation is dominant or surface nucleation is negligible, the contribution of the number of volume nuclei compared to that of the surface nuclei to the total number of nuclei in the sample also increases with increasing particle size and $(\delta T)_p$ increase.

The crystal growth dimension, n, given by [16]

$$n = 2.5(R/E)\left[T_p^2/(\Delta T)_p\right] \qquad (2)$$

is frequently used for describing surface or volume crystallization in glasses. Here, R is the gas constant and E the effective activation energy for the glass-to-crystal transformation. Assuming E to be independent of particle size and temperature (at least in the temperature regime of the DTA scans), the ratio $T_p^2/(\Delta T)_p$ was also used as a qualitative measure for evaluating the crystallization mechanism of glass powders. If surface crystallization continues to dominate with increasing particle size, $T_p^2/(\Delta T)_p$ should be the same for all particle sizes. Crystal growth on volume nuclei results in a three-dimensional crystallization process. For dominant volume crystallization, therefore, $T_p^2/(\Delta T)_p$ should increase with increasing particle size.

DTA curves of samples with granulations ranging from <0.038–1 mm were recorded at a heating rate of $v = 10$°C/min to determine the dominant crystallization mechanism. All the DTA curves had two exothermal peaks, Fig. 1. Peak 1 appears at a lower temperature

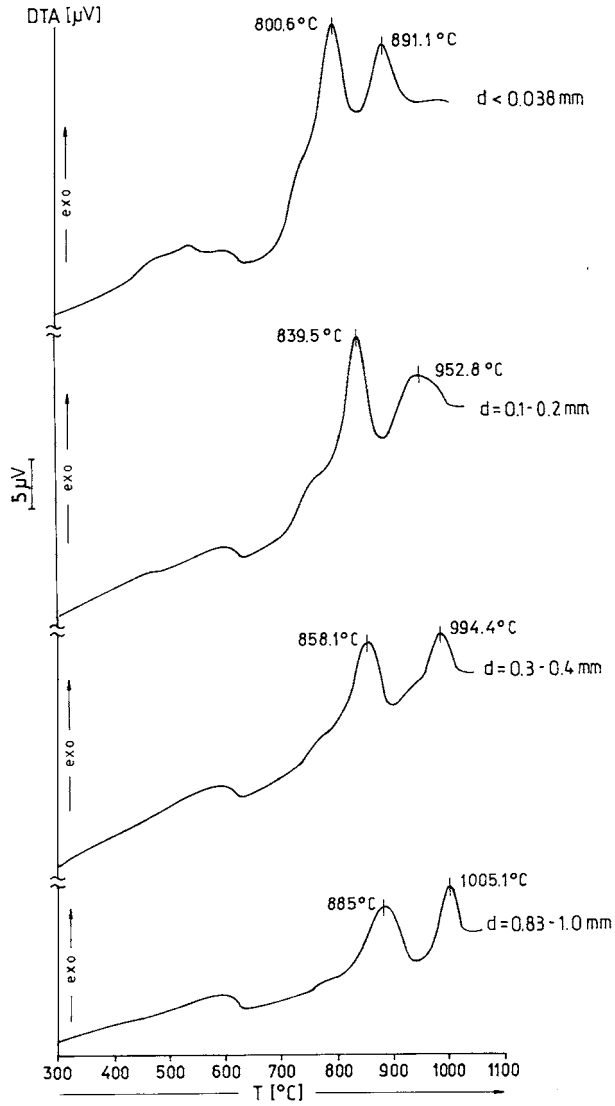

Figure 1 DTA traces recorded at a heating rate of 10°C/min for particle sizs <0.038; 0.1–0.2; 0.3–0.4 and 0.83–1.0 mm.

range $T_{p1} = 800.6$–885°C, while peak 2 appears at a higher temperature interval $T_{p2} = 891$–1005.1°C. Additionally, dilatometric measurements indicate that this glass has a transformation temperature at $T_g = 618$°C. On the basis of these results it may be concluded that the temperature interval of nucleation and crystal growth vary considerably. Therefore, the selection of low heating rates enables that a certain number of nuclei be formed in the glass transformation region where the nucleation rates are significant and the crystal growth rates are negligible. This number of nuclei does not significantly change with further heating in the higher temperature interval because the nucleation rates in this range are low, while the crystal growth rates become considerable. That is why crystal growth in this glass proceeds at a constant number of nuclei under non-isothermal conditions.

The behavior of the crystallization peaks with varying powder particle size is different. Fig. 1 shows examples of DTA curves for four samples of different particle size where such behavior of peaks 1 and 2 is illustrated. In the case of peak 1, the peak height decreases with increasing particle size, while the peak width and temperature increase. The behavior of peak 2 is more

complex and three different regions are registered. In the particle size range <0.038–0.1 mm, the height of peak 2 decreases while the peak width and temperature increase. In the particle size range 0.1–0.5 mm, the width of peak 2 decreases while the peak height and temperature increase. For particle sizes 0.5–1 mm, the peak width also decreases, the peak height increases and the peak temperature remains almost constant.

In order to identify the crystal phases that are formed at the temperatures corresponding to peak 1 and 2, two groups of experiments were performed under isothermal conditions with samples of particle size presented in Fig. 1. The first group of samples was heated at a rate of $v = 10^{\circ}$C/min to the temperature of peak 1 for each chosen granulation. Upon reaching this temperature, they were treated for $t = 15$ min. The second group of samples of the same granulation was heated to the temperature of peak 2, specific for each chosen granulation and then treated for the same time. The XRD diffractograms of these samples are presented in Figs 2 and 3. The basic characteristic of the patterns shown in Fig. 2 is the presence of a considerable amount of amorphous substance and the crystalline β-$Ca_2P_2O_7$ (C) phase. The $Ca_2P_2O_7$ phase appears in several different polymorphs (α, β, γ) [17]. To define the polymorphic form which is formed at this composition, bulk samples were used which were thermally treated in a two-stage regime under the conditions presented in Table II. Careful examination of numerous samples did not reveal the crystallization of other known $Ca_2P_2O_7$ polymorphs (α or γ) or the metastable phase discussed in the paper of Nan *et al*. [8]. Table III shows the calculated unit cell parameters for the β-$Ca_2P_2O_7$ phase of a sample in an early stage of crystallization ($T_c = 770^{\circ}$C for $t = 1800$ min), medium stage of crystallization ($T_c = 830^{\circ}$C for $t = 1200$ min) and of a sample that has no amorphous phase ($T_c = 1100^{\circ}$C for $t = 600$ min). It is obvious that the calculated values are somewhat higher than the corresponding ones given for a standard JCPDS pattern (33–0297). The nature of these differences could be connected either to isomorphous replacement of Ca^{2+} by Ti^{4+} and Al^{3+} cations in the β-$Ca_2P_2O_7$ lattice or to the microstructural parameters of this phase. The first possibility is less probable because of the significant differences in the size of the ionic radii of the denoted cations. Preliminary investigations of the change of the microstructural parameters indicate that changes in the values of the unit cell of the β-$Ca_2P_2O_7$ phase are a consequence of the arrangement of the crystal lattice and will be published separately.

Fig. 3 shows the diffractograms of powder samples crystallized at the temperature of peak 2. Besides the previously identified β-$Ca_2P_2O_7$ phase, the patterns are characterized by the appearance of TiP_2O_7, $AlPO_4$ (JCPDS card files 38-1468 and 31-0028, respectively) and minor amounts of amorphous substance. The unit cell obtained for the TiP_2O_7 phase, Table IV, are greater than those published by McMurdie *et al*. [18]. The reasons for these differences could be explained in the

TABLE II Results of investigating the crystallization mechanism under isothermal conditions

T_c(°C)[a]	T_c(min)	Mechanism of crystallization	Phase composition
770	600	—	G
	6000	Surface	G + C
	9000	Volume	G + C + T + A
830	600	Surface	G + C
	1200	Surface	G + C
	4800	Volume	G + C + T + A
860	30	Surface	G + C
	120	Volume	G + C + T + A
900	15	Surface	G + C
	45	Volume	G + C + T + A
960	20	Volume	G + C + T + A
1000	15	Volume	G + C + T + A
1100	600	Volume	C + T + A

[a]In all the experiments the samples were treated at: $T_n = 690^{\circ}$C for $t_n = 600$ min before crystallization.
G-Glass; C-Calcium Pyrophosphate (β-$Ca_2P_2O_7$); T-Titanium Phosphate (TiP_2O_7); A-Aluminium Phosphate ($AlPO_4$).

TABLE III Changes of the unit cell parameters of the β-$Ca_2P_2O_7$ phase synthesized under different temperature/time conditions

T_c (°C)/t (min)	a (Å)	c (Å)	V (Å)
770/1800	6.700(1)	24.106(7)	1082.1(4)
830/1200	6.6874(9)	24.139(6)	1079.5(3)
1100/600	6.6852(9)	24.142(5)	1078.9(3)
JCPDS 33-0297	6.684(6)	24.145(15)	1078.5

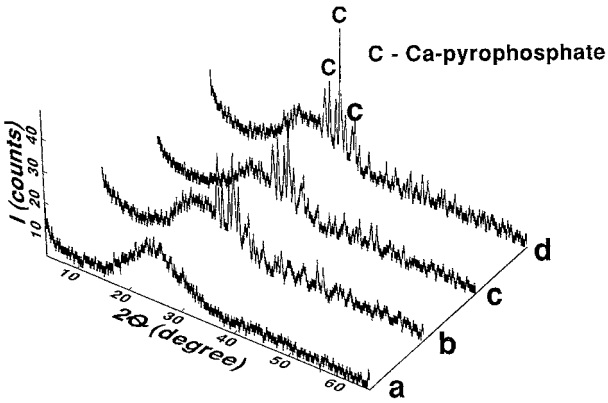

Figure 2 XRD patterns of (a) the initial glass and of powder samples of particle size: (b) <0.038 mm, annealed at $T_c = 800^{\circ}$C, (c) 0.1–0.2 mm, annealed at $T_c = 840^{\circ}$C and (d) 0.83–1.0 mm, annealed at $T_c = 885^{\circ}$C.

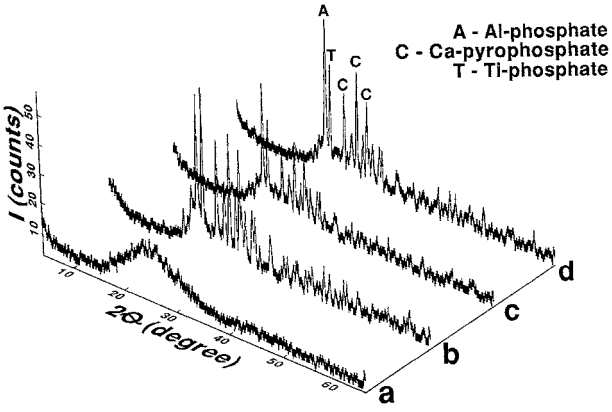

Figure 3 XRD patterns of (a) the initial glass and of powder samples of particle size, (b) <0.038 mm, annealed at $T_c = 891^{\circ}$C, (c) 0.1–0.2 mm, annealed at $T_c = 953^{\circ}$C and (d) 0.83–1.0 mm, annealed at $T_c = 1005^{\circ}$C.

TABLE IV The most important crystallographic parameters for the crystalline phases, obtained by Rietveld (profile matching mode) refinement of the XRD pattern

Phase	Unit cell dimension		Reliability factors		
	a (Å)	c (Å)	R_B (%)	R_f (%)	Common
β-$Ca_2P_2O_7$	6.6899(1)	24.1558(3)	2.68	1.47	$R_p = 10.01$;
TiP_2O_7	23.6424(2)		4.15	1.76	$R_{wp} = 14.12$;
$AlPO_4$	7.207[a]		3.67	1.772	$R_{exp} = 9.64$; Chi = 2.67

[a]Not refined.

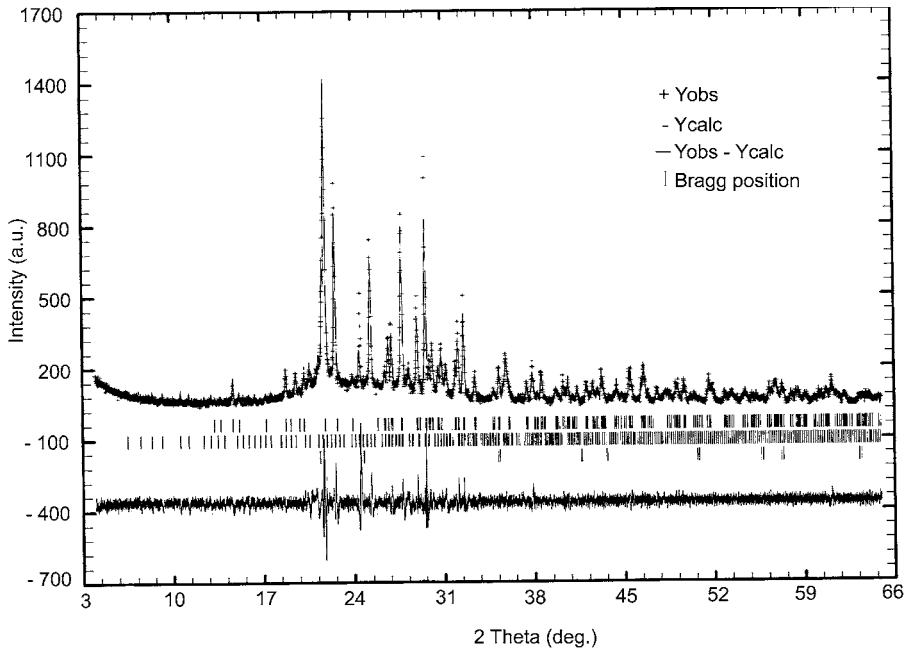

Figure 4 Rietveld refinement plot of a glass sample heat treated at: $T_n = 690°C$ for $t = 600$ min and $T_c = 1100°C$ for $t = 600$ min.

same way as discussed for the β-$Ca_2P_2O_7$ phase. However, it is important to notice that the crystal structure of the TiP_2O_7 phase is not well known As seen from Table IV, problems were encountered to refine the $AlPO_4$ phase. This phase is characterized by a very strong peak near 4.1 Å, characteristic for a cristobalite stuffed derivative. Consequently, it was treated in the Rietveld refinement as a cubic (JCPDS card 31-0028) phase with $a = 7.207$ Å. Due to the very low intensities of the other peaks and their overlapping with reflections of the other two phases present in the analyzed powder pattern, the Rietveld refinement missed. A Rietveld profile matching mode fitting plot of the sample not containing the amorphous phase (1100°C/600 min, Table II) is presented in Fig. 4, while the results of the fitting are shown in Table IV. The semi-quantitative estimation shows that the tetrahedral β-$Ca_2P_2O_7$ phase is the most abundant one, while the amount of the cubic TiP_2O_7 phase is greater than that of the cubic $AlPO_4$ one. These results indicate that $Ca_2P_2O_7$ is formed at peak 1, while the phases TiP_2O_7 and $AlPO_4$ are formed at peak 2 in the case of all particle sizes from <0.038–1.0 mm.

Figs 5 and 6 show the analysis of the influence of particle size on peak temperature, T_p, peak width at peak half height $(\Delta T)_p$, peak height $(\delta T)_p$ and the ratio $T_p^2/(\Delta T)_p$ for both peaks. It may be seen from these figures that the temperature T_p increases with increasing size for both peaks (curves a_1 and a_2). The behavior of parameter $(\Delta T)_p$ for peaks 1 and 2 is different. In the case of peak 1, $(\Delta T)_p$ increases with increasing particle size (curve b_1). In the case of peak 2 the behavior of parameter $(\Delta T)_p$ is considerably more complex (curve b_2). The peak height $(\delta T)_p$ and ratio $T_p^2/(\Delta T)_p$ decrease with increasing particle size in the case of peak 1 (curves c_1 and d_1). The behavior of these parameters for peak 1 is in accordance with theoretical predictions for the case of the predominant surface mechanism of crystallization. In that case the surface nuclei dominate in the total number of nuclei. The ratio of particle surface to volume decreases with increasing particle size, as does the number of surface nuclei, i.e., the total number of nuclei. Consequently, the parameters $(\delta T)_p$ and $T_p^2/(\Delta T)_p$ also decrease. In the case of peak 2 the behavior of these two parameters is much more complex (curves c_2 and d_2). Both parameters decrease with increasing particle size to the size of 0.15 mm at which they attain a minimum. In the size interval 0.15–0.5 mm both parameters increase to an asymptotic value, while in the size range greater than 0.5 mm both parameters remain approximately constant. Such behavior is in accordance with theoretical predictions for the case when the volume one, at constant phase composition is replacing the surface mechanism of crystallization. In that case in the particle size range 0–0.15 mm the number of surface nuclei dominates in the total number

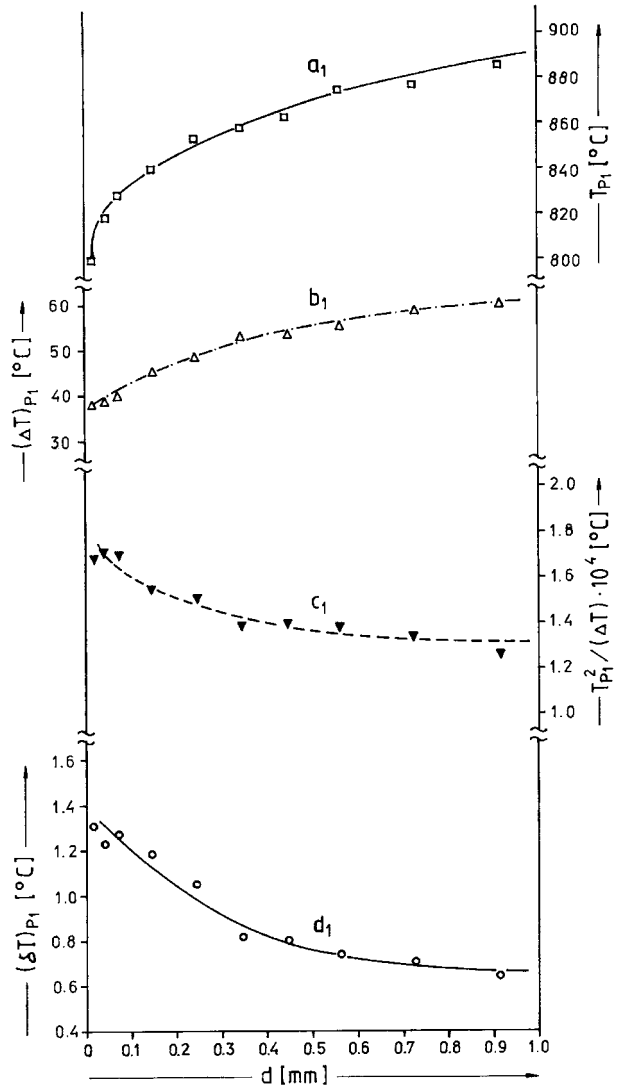

Figure 5 Effect of particle size on DTA peak 1 (a) the temperature T_p; (b) the width at half height $(\Delta T)_p$, (c) the ratio $T_p^2/(\Delta T)_p$ and (d) the height $(\delta T)_p$.

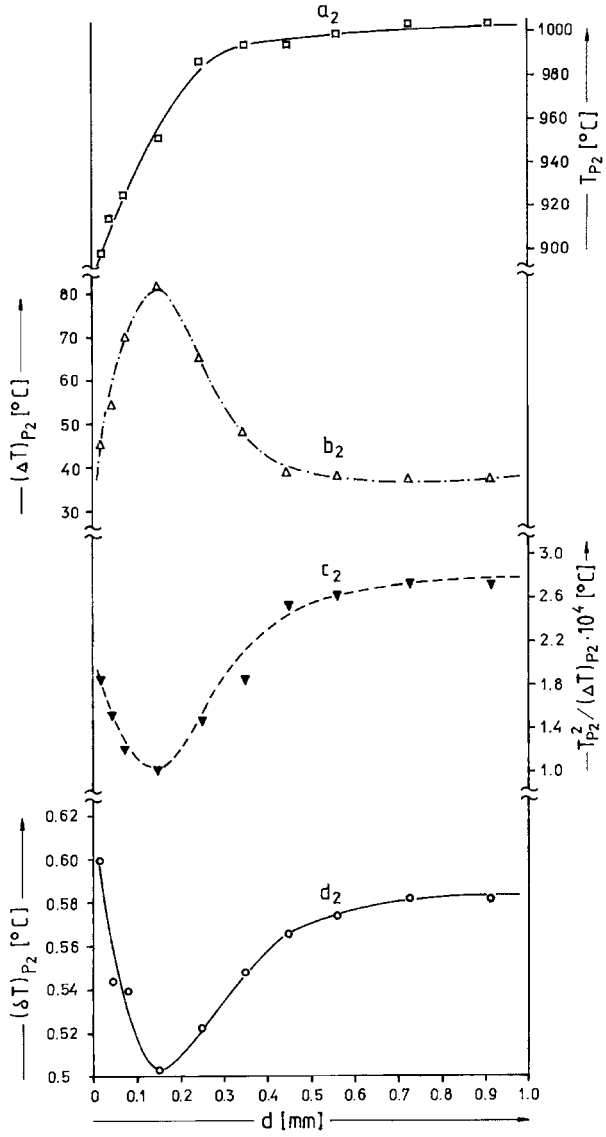

Figure 6 Effect of particle size on DTA peak 2 (a) the temperature T_p, (b) the width at half height $(\Delta T)_p$, (c) the ratio $T_p^2/(\Delta T)_p$ and (d) the height $(\delta T)_p$.

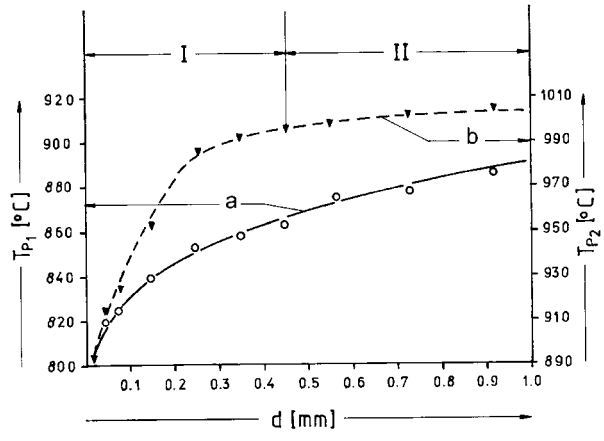

Figure 7 Behavior of the temperature peak T_p for: (a) a surface and (b) a volume mechanism of crystallization.

of nuclei, as does the surface mechanism of crystallization. In the size range 0.15–0.50 mm the number of surface nuclei continues to decrease due to the decrease in the particle surface to volume ratio. The volume of the particles increases together with their size, as does the number of volume nuclei and they gradually start to dominate. Consequently, the total number of nuclei increases as do the parameters $(\delta T)_p$ and $T_p^2/(\Delta T)_p$. Both mechanisms of crystallization are present in this range. In the size range >0.5 mm the number of volume nuclei dominates in the total number of nuclei so the volume crystallization mechanism prevails. Further increase of the particle size and volume does not significantly increase the number of volume nuclei or the total number of nuclei. Therefore, both parameters $(\delta T)_p$ and $T_p^2/(\Delta T)_p$ remain approximately constant in this size range and the volume mechanism of crystallization is dominant.

Fig. 7 shows a comparative presentation of the change in T_p for peaks 1 and 2. It may be clearly seen from the figure that the increase of T_{p2} is stronger than that of T_{p1} in range I and the opposite in range II. Such behavior of the crystallization peak temperatures may be explained by the influence of different crystallization mechanisms of the glass. As the surface crystallization mechanism is operational at T_{p1}, the particle surface and the number of surface nuclei decrease with increasing particle size. Consequently, T_{p1} and the glass resistance to crystallization increase in the whole

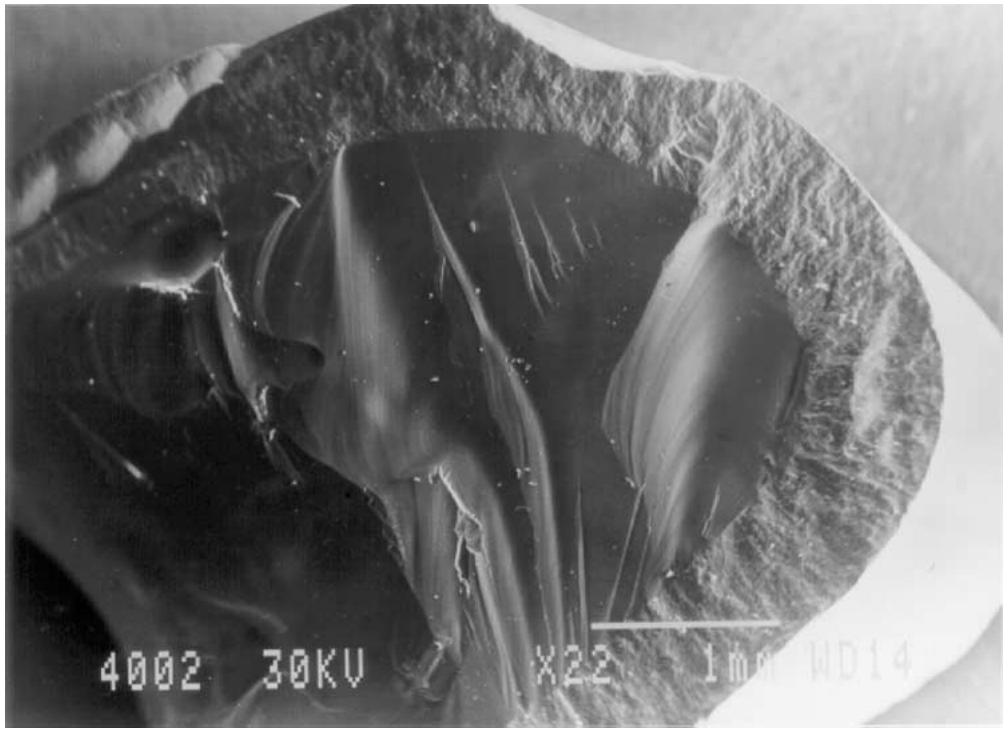

(a)

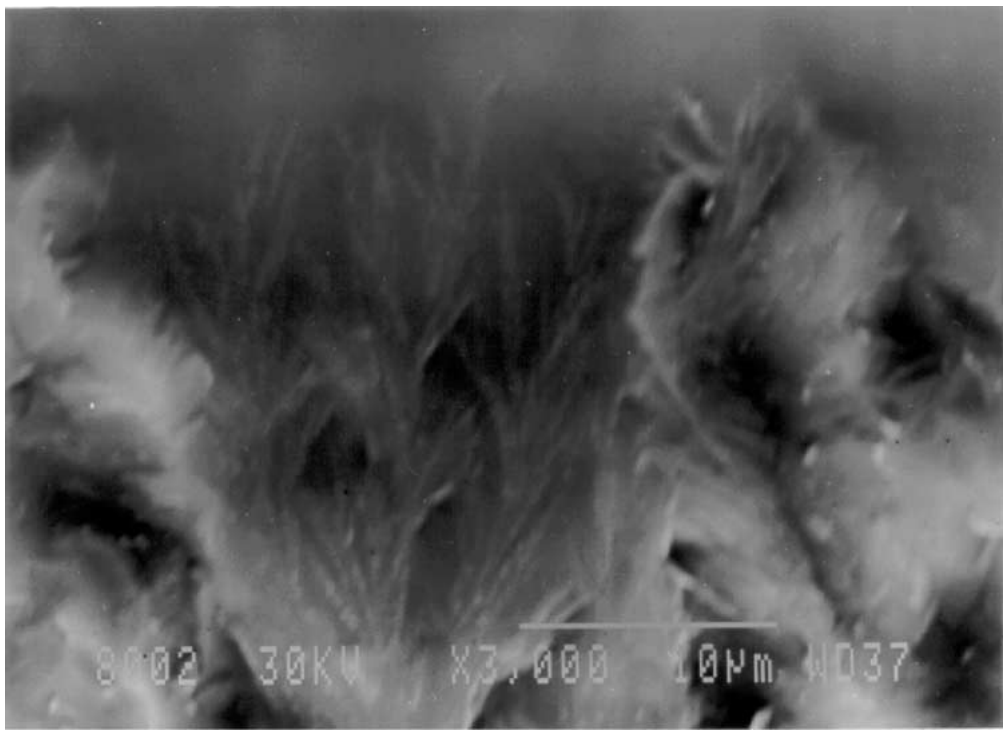

(b)

Figure 8 SEM micrographs of samples with the following heat treatments: $T_n = 690°C$ for $t = 600$ min and $T_c = 770°C$ for $t = 1800$ min: (a) crystallized surface layer and (b) interface crystals-glass at higher magnification.

particle size range 0–1 mm. In the case of peak 2 the increase of T_{p2} is greater than that of T_{p1} in range I (0–0.5 mm), where the surface mechanism of crystallization is dominant or both mechanisms are equally likewise effective. In this range the number of surface nuclei decreases with increasing particle size and the number of volume nuclei is still not sufficiently significant, so T_{p2} and the glass resistance to crystallization greatly increase. When the number of volume nuclei is dominant, range II (0.5–1 mm), increasing particle size does not significantly influence the change in the number of volume, so T_{p2} and the glass resistance to crystallization do not change relevantly.

To confirm the complex crystallization behavior of this glass, additional experiments were performed under isothermal conditions. The results of these investigations are presented in Table II. In these experiments bulk samples were thermally treated at the nucleation temperature $T_n = 690°C$ for $t = 10$ h and then at a crystallization temperature in the interval $T_c = 770$–$1100°C$

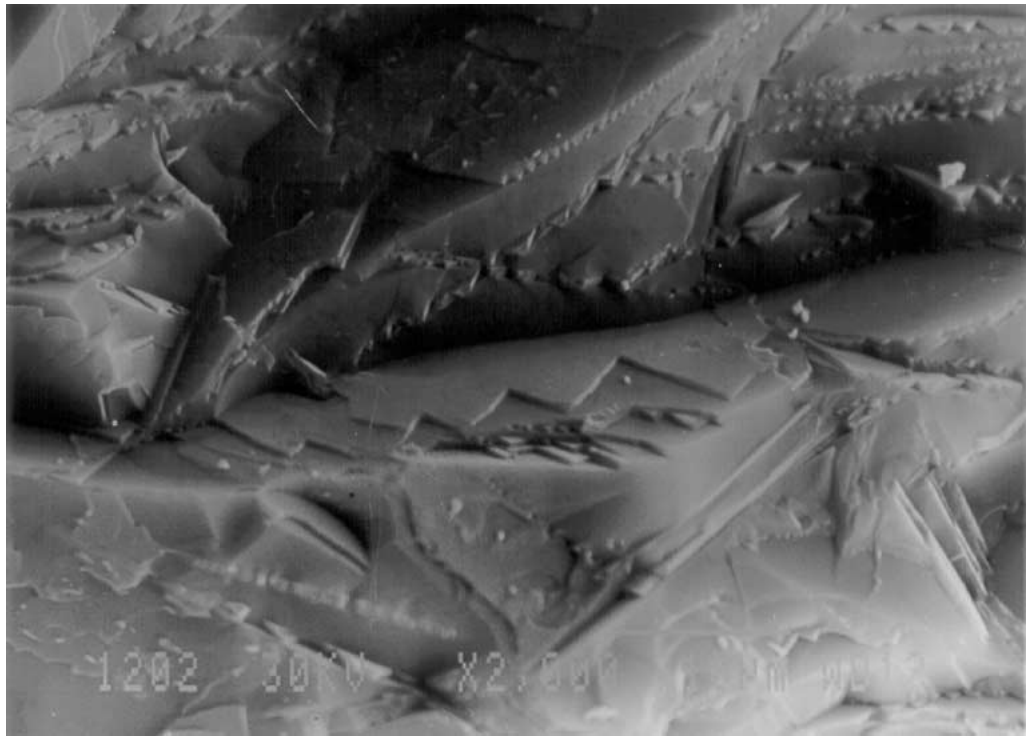

Figure 9 SEM micrographs of samples with the following heat treatments: $T_n = 690^\circ C$ for $t = 600$ min and $T_c = 900^\circ C$ for $t = 45$ min.

for various times. The nucleation temperature (T_n) was determined in experiments which will be published separately. Such an experimental regime enables the crystal growth to take place at a constant number of nuclei which, in the case of this glass, also corresponds to crystallization under non-isothermal conditions. It may be seen from Table II that at crystallization temperatures in the range $T_c = 800$–$900^\circ C$ surface crystallization is initially detected and the β-$Ca_2P_2O_7$ phase is formed. By increasing the annealing time, the thickness of the surface crystallized layer grows and the growth morphology of these crystals is dendritic, Fig. 8a and b. Also, these results indicate that long annealing times are required for the appearance of volume crystallization. Thus, at $T_c = 770^\circ C$ at annealing times shorter than 30 h the glass does not crystallize. A surface crystalline layer starts to form at an annealing time of $t = 30$ h. At an annealing time of $t = 150$ h volume crystallization is detected, as well as the appearance of the TiP_2O_7 and $AlPO_4$ phases. However, the crystal growth rates of these phases are so low that even after an annealing time of 200 h the sample contains a significant amount of glass. With increasing T_c the annealing time till the appearance of volume crystallization decreases. At $T_c = 860^\circ C$ the appearance of volume crystallization was registered after an annealing time of $t = 62$ h. At $T_c > 900^\circ C$ only volume crystallization was detected and all three phases (β-$Ca_2P_2O_7$, TiP_2O_7 and $AlPO_4$) were identified, Fig. 9. These results indicate that the additives TiO_2 and Al_2O_3 at this composition do not influence the nucleation of the β-$Ca_2P_2O_7$ phase, because it is also formed in their presence by the surface crystallization mechanism. The presence of TiO_2 and Al_2O_3 enables only nucleation for the formation of the TiP_2O_7 and $AlPO_4$ phases at volume crystallization. Also, as the number of nuclei in these experiments was constant, these results show that the reason for the appearance of two temperature peaks in the DTA curve is the large difference in the crystal growth rates of these three phases. In the temperature range $T < 900^\circ C$, the crystal growth rate of the β-$Ca_2P_2O_7$ phase is considerably higher than the ones of TiP_2O_7 and $AlPO_4$ phases. Consequently, peak 1 appears in this temperature range in which only the β-$Ca_2P_2O_7$ phase was identified and the glass powder crystallizes by the surface crystallization mechanism in the whole particle size range 0–1 mm. At $T > 900^\circ C$ the crystal growth rates of the TiP_2O_7 and $AlPO_4$ phases attain the crystal growth rate of the β-$Ca_2P_2O_7$ phase. Peak 2 appears and the TiP_2O_7 and $AlPO_4$ phases were also identified.

4. Conclusion

The topic of these investigations was the crystallization behavior of calcium phosphate glass powder with the molar ratio $[CaO]/[P_2O_5] = 0.88$ which contained 6.38 mol% TiO_2 and 10 mol% Al_2O_3. The crystallization of this glass was detected in DTA curves as two successive exothermal peaks which differ by about $90^\circ C$ and appear in the temperature interval 800–$1000^\circ C$. The results of the investigation show complex crystallization behavior of the glass powder which depends on the particle size and crystallization temperature.

In the temperature range of crystallization $T_c < 900^\circ C$:

- the surface mechanism of crystallization predominates for all particle sizes from 0–1 mm and the β-$Ca_2P_2O_7$ phase is formed,
- with increasing particle size there is a trend of an increase of the crystallization temperature and of the glass resistance to crystallization,

– at very long annealing times in this temperature interval volume crystallization occurs and the TiP_2O_7 and $AlPO_2$ phases are formed.

In the temperature interval of crystallization $T_c > 900°C$:

– the surface mechanism of crystallization is dominant in the case of particle sizes <0.15 mm,
– in the size range 0.15–0.50 mm the surface mechanism of crystallization is replaced by the volume one,
– in the size range >0.5 mm the volume mechanism of crystallization is dominant,
– the β-$Ca_2P_2O_7$, TiP_2O_7 and $AlPO_4$ phases appear in the case of all particle sizes,
– in the particle size range <0.5 mm there are sharply increasing trends of the crystallization temperature peak and of the glass resistance to crystallization. For particle sizes greater than 0.5 mm, the temperature of the crystallization peak and the resistance to crystallization do not significantly change with varying particle size,
– TiO_2 and Al_2O_3 in this composition influence the nucleation and formation of the TiP_2O_7 and $AlPO_4$ phases and in this manner change the crystallization mechanism of this glass from the surface to the volume mechanism. They do not influence the nucleation and formation of the β-$Ca_2P_2O_7$ phase,
– analyses also indicate that there is a large difference in the crystal growth rates of these phases in various temperature intervals.

References

1. R. K. BROW, *J. Non-Cryst.Solids*, **263/264** (2000) 1.
2. U. HOPPE, *ibid.* **195** (1996) 138.
3. U. HOPPE, G. WALTER, A. BRAZ, D. STACHEL and A. C. HANNON, *J.Phys.: Condens. Matter.* **10** (1998) 261.
4. W. VOGEL and W. HÖLAND, *Angw.: Chem. Int. Ed. Engl.* **26** (1987) 527.
5. P. F. JAMES, Y. IQBAL, U. S. JAIS, S. JORDERY and W. E. LEE, *J. Non-Cryst. Solids* **219** (1997) 17.
6. A. WATANABE, M. MISUDOU, S. KIHARA and Y. ABE, *J. Amer. Ceram. Soc.* **72** (1989) 1499.
7. H. HOSONO, Z. ZHANG and Y. ABE, *ibid.* **72** (1989) 1587.
8. Y. NAN, W. E. LEE and P. F. JAMES, *ibid.* **75** (1992) 1641.
9. I. M. REANEY, P. F. JAMES and W. E. LEE, *ibid.* **79** (1996) 1934.
10. M. B. TOŠIĆ, M. M. MITROVIĆ and R. Z. DIMITRIJEVIĆ, *J. Mater. Sci.* **35** (2000) 3659.
11. U. HOPPE, G. WALTER, R. KRANOLD and D. STACHEL, *J. Non-Cryst. Solids* **263/264** (2000) 29.
12. P. HARTMANN, J. VOGEL, U. FRIEDRICH and C. JÄGER, *ibid.* **263/264** (2000) 94.
13. C. S. RAY, Q. YANG, W. HAUNG and D. E. DAY, *J. Amer. Ceram. Soc.* **79** (1996) 3155.
14. A. MAROTTA, A. BURI and F. BRANDA, *J. Mater. Sci.* **16** (1981) 341.
15. K. F. KELTON, K. LAKSHMI NARAYAN, L. E. LEVINE, T. C. CULL and C. S. RAY, *J. Non-Cryst. Solids* **204** (1996) 13.
16. J. A. AUGIS and J. E. BENNETT, *J. Thermal. Anal.* **13** (1978) 283.
17. N. C. WEBB, *Acta Crystallogr.* **21** (1966) 942.
18. H. MCMURDIE *et al.*, *Power Diffraction* **2** (1987) 52.

Received 13 November 2001
and accepted 3 July 2002